ARTICLE

Tumor Targeting and Imaging in Live Animals with Functionalized Semiconductor Quantum Rods

Ken-Tye Yong,[†] Rui Hu,[†] Indrajit Roy,[†] Hong Ding,[†] Lisa A. Vathy,[†] Earl J. Bergey,[†] Masamichi Mizuma,[‡] Anirban Maitra,[‡] and Paras N. Prasad*[,†]

Institute for Lasers, Photonics and Biophotonics, The State University of New York at Buffalo, Buffalo, New York 14260-4200, Department of Pathology and Oncology, The Sol Goldman Pancreatic Cancer Research Center, CRB-2, Suite 345, Johns Hopkins University School of Medicine, 1550 Orleans Street, Baltimore, Maryland 21231

ABSTRACT In this contribution, we demonstrate that highly luminescent CdSe/CdS/ZnS quantum rods (QRs) coated with PEGylated phospholipids and conjugated with cyclic RGD peptide can be successfully used for tumor targeting and imaging in live animals. The design of these targeted luminescent probes involves encapsulation of hydrophobic CdSe/CdS/ZnS QRs with PEGylated phospholipids, followed by conjugation of these PEGylated phospholipids to ligands that specifically target the tumor vasculature. In vivo optical imaging studies in nude mice bearing pancreatic cancer xenografts, both subcutaneous and orthotopic, indicate that the QR probes accumulate at tumor sites via the cyclic RGD peptides on the QR surface binding to the $\alpha_v\beta_3$ integrins overexpressed in the tumor vasculature, following systemic injection. In vivo tumor detection studies showed no adverse effects even at a dose roughly 6.5 times higher than has been reported for in vivo imaging studies using quantum dots. Cytotoxicity studies indicated the absence of any toxic effect in the cellular and tissue levels arising from functionalized QRs. These results demonstrate the vast potential of QRs as bright, photostable, and biocompatible luminescent probes for the early diagnosis of cancer.

KEYWORDS: quantum rods • bioimaging • bioconjugation • targeted delivery • pancreatic cancer • peptide

INTRODUCTION

One-dimensional semiconductor nanostructures such as quantum wires (1−7) and quantum rods (QRs) (8, 9) have been attracting significant interest over the past decade because of their tunable optical properties, which, in turn, give rise to applications in biomedical fields ranging from multiplex imaging to sensors (7, 10−17). Recently, a wide array of methods in manipulating the shape and size of CdSe nanocrystals (NCs) have been reported (18). For example, CdSe QRs were prepared by solution techniques using structure-directing agents (19), metallic nanoparticles (20), micellar templating techniques (21), etc. (5, 22−25). The controlled synthesis of NCs with various shapes is an important step in the development of ultrasensitive targeted probes for cancer research applications especially for early cancer detection (26, 27). CdSe QRs have several advantages that make them potentially much better bioprobes in comparison to spherical quantum dots (QDs) (28). These include a larger absorption cross section and a larger surface area per particle, which facilitates conjugation with multiple active molecules (e.g., probes for other imaging modalities, therapeutic molecules, biorecognition molecules for target specificity, etc.) (29). Their Stokes shift is strongly dependent on the aspect ratio (length/diameter) of the rod (30). The emission of single QRs can be reversibly switched on and off by externally applied electric fields. Also, it was reported that CdSe QRs emitted light that was linearly polarized along the *c* axis of the crystallites and that the degree of polarization was dependent on the aspect ratio of the NCs (31). Interestingly, despite these several advantages associated with QRs, investigations on their use in bioimaging only recently started, promoted by the advancement of well-controlled synthesis and surface functionalization approaches. Recently, Alivisatos' and our group have demonstrated live in vitro cancer cell imaging using CdSe/CdS/ZnS QRs as targeted luminescent probes (32, 33). Both studies have shown the advantages of QRs as biocompatible targeted imaging probes. Alivisatos' group has demonstrated that QRs are brighter single-molecule probes than QDs. Our group has shown that these QRs can be used for two-photon luminescence imaging of cancer cells in vitro with reduced photodamage, as compared to UV−vis light excited single photon imaging.

Poly(ethylene glycol)-grafted (PEGylated) phospholipids in aqueous media self-assemble into polymeric micelles with diameters generally smaller than 80 nm. Phospholipid micelles are more stable than detergent micelles and have very low critical micelle concentration values ($\sim 10^{-6}$ M). Similar to detergent micelles, polymeric micelles solubilize "oil-like" particles by incorporating them into their hydrophobic core. More importantly, the outer surface of phospholipid micelles displays a dense layer of PEG that is nonimmunogenic. This favors reduced capture and degradation by the reticuloendothelial system (RES) and yielded extended systemic cir-

* E-mail: pnprasad@buffalo.edu.
Received for review December 11, 2008 and accepted February 13, 2009
[†] The State University of New York at Buffalo.
[‡] Johns Hopkins University School of Medicine.
DOI: 10.1021/am8002318

Published on Web 03/10/2009

culation time, broad biodistribution, and lowered toxicity of the encapsulated nanoparticles. In addition, the PEG lipids can be further functionalized with specific reactive groups (e.g., carboxyl, amine, and maleimide) for conjugation purposes. Though micellar encapsulation of QDs has been demonstrated (34), we are not aware of any previous reports of producing high-quality water-dispersible CdSe/CdS/ZnS QRs using phospholipid micelles for in vivo tumor targeting and imaging.

It is well-known that new blood vessels (neovasculature) form around growing tumors in order to meet their demand of high nutrient supply, a process known as angiogenesis (35). To achieve this, the endothelial cells surrounding tumor tissue organize themselves into capillaries that are attached to the extracellular matrix (ECM). Integrins such as $\alpha_V\beta_3$ are cell-surface receptors that anchor these endothelial cells to the ECM and transduce signals from the extracellular environment to the cell's interior. During angiogenesis, the $\alpha_V\beta_3$ integrins are known to be overexpressed on the surface of the endothelial cells surrounding tumor tissues. In addition, this integrin also plays a critical role in the invasion, metastasis, and proliferation of the tumor (36). Therefore, the $\alpha_V\beta_3$ integrin serves as an extremely potent target from the point of view of the development of novel diagnostic and therapeutic probes that would specifically "home in" on tumor sites in vivo. Of special interest is the triplet peptide Arg-Gly-Asp (RGD), which is known to specifically bind to the $\alpha_V\beta_3$ integrins overexpressed on the tumor endothelium, thus serving as an antagonist against vascular endothelial cells and tumor growth (37). In addition to their potential role as a therapeutic molecule, RGD peptides modified with an imaging probe can also be used as a diagnostic tool to image $\alpha_V\beta_3$ integrin expression on developing tumors (38). In this regard, QRs bioconjugated with RGD peptides, owing to their high luminescence, can potentially play a critical role toward the diagnosis of developing tumors in vivo via noninvasive optical imaging. In addition to preoperative/therapeutic diagnosis, the QR-labeled RGD peptides can also be used for image-guided surgery because they can delineate tumor margins from normal tissues during surgery. Thus, QR-labeled RGD peptides could be used as a new class of tumor (i.e., tumor angiogenesis) specific marker in cancer detection (39).

In this work, we aimed to first provide a "proof of principle" demonstration of in vivo tumor targeting and imaging using cyclic RGD (cRGD)-peptide-conjugated CdSe/CdS/ZnS QRs. These CdSe/CdS/ZnS QRs were first stably dispersed in an aqueous solution by encapsulation within PEGylated and functionalized phospholipid micelles, a strategy that provided not only PEG molecules on the QR surface for their enhanced colloidal stability in physiological circulation but also active groups for an easy conjugation of synthetic cRGD peptides for tumor-specific delivery. Following systemic injection of this QR formulation in mice bearing pancreatic cancer xenografts, we have demonstrated successful in vivo tumor labeling using a whole body live animal optical imaging system, where the QR-targeted tumor can be easily distinguished from the background tissues (skin, hair, and food). This tumor imaging was demonstrated in mice bearing not only subcutaneously inoculated tumor xenografts but also the more biologically relevant orthotopically implanted tumor xenografts. Furthermore, our biodistribution and cellular toxicity studies involving these highly luminescent QR-based probes in live animals indicated the absence of any observable toxicity, indicating biocompatibility of these nanoprobes. These results underscore the potential of QRs as ultrasensitive and biocompatible optical probes for the early diagnosis of cancer and other diseases.

EXPERIMENTAL SECTION

Materials and Methods. A. ***Materials.*** Cadmium oxide, zinc acetate, sulfur, selenium, trioctylphosphine oxide (TOPO), trioctylphosphine (TOP), oleic acid, and high-performance liquid chromatography (HPLC) water were purchased from Aldrich. Tetradecylphosphonic acid (TDPA) is a product of Alfa Aesar. RGD peptides (PCI-3686-PI) were purchased from Peptides International, Inc. All chemicals were used as received. All solvents (hexane, toluene, and ethanol) were of reagent grade and were used without further purification.

B. ***Typical Synthesis Procedures. (i) Synthesis of CdSe QRs.*** The following protocol was adopted from our previous report (33) to obtain CdSe QRs. A total of 1.6 mmol of cadmium oxide, 3 mmol of TDPA, and 3 g of TOPO were loaded into a 100 mL three-necked flask. Next, the reaction mixture was slowly heated under an argon atmosphere to 290−300 °C. After 10−15 min of heating, a clear homogeneous solution was obtained. The reaction mixture was maintained at 300 °C for another 5 min, and then 0.8 mL of 1 M TOP-Se was rapidly injected. The reaction was stopped after 2−3 min by removing the heating mantle. The QRs were separated from the surfactant solution by the addition of ethanol and centrifugation. The reddish QR precipitate could be readily redispersed in various organic solvents (hexane, toluene, and chloroform).

(ii) Synthesis of CdSe/CdS/ZnS QRs with an Aspect Ratio of ∼4.6. The synthesis method of forming a CdS/ZnS graded shell on CdSe QR was adapted from Manna et al. (40). A CdSe QR solution was prepared in advance by dissolving ∼0.3 g of CdSe QRs in ∼5 mL of toluene. Separately, 2 mmol of cadmium oxide, 4 mmol of zinc acetate, and 5.5 g of TOPO were dissolved in 10 mL of oleic acid. The reaction mixture was heated to 180 °C for ∼30 min under an argon flow, and then the CdSe nanorod solution was injected slowly under stirring into the hot reaction mixture. The reaction mixture was held at 180 °C, with a needle outlet that allowed the toluene to evaporate. After ∼15 min of heating, the needle was removed, and the reaction temperature was raised to 210 °C. When the desires temperature was reached, 2 mL of TOP-S was added dropwise into the reaction mixture. The reaction mixture was then held at ∼210 °C for 10−15 min, and then an aliquot was removed via syringe and was injected into a large volume of toluene at room temperature, thereby quenching any further growth of the QRs. The QRs were separated from the toluene solution by the addition of ethanol and centrifugation.

C. ***Preparation of Phospholipid-Micelle-Encapsulated QRs.*** The as-prepared organic-dispersible QRs were separated from by the addition of ethanol (volume ratio of QRs to ethanol 1:3) and centrifugation (12 000 rpm for 20 min). The precipitate was collected and dried in vacuo and redispersed in chloroform. Next, QRs dispersed in chloroform (∼3 mg/mL), DSPE-mPEG (1,2-diacyl-*sn*-glycero-3-phosphoethanolamine-*N*-[methoxy[poly-(ethylene glycol)]], average MW 5000, catalog no. mPEG-DSPE-5000-1g, Laysan Bio, Inc.) in a chloroform solution (∼10 mg/

mL) and DSPE-PEG-maleimide (1,2-distearoyl-*sn*-glycero-3-phosphoethanolamine-*N*-[maleimide[poly(ethylene glycol)], ammonium or sodium salt, average MW 3400, catalog no. DSPE-PEG-MAL-3400-1g, Laysan Bio, Inc.) in a chloroform solution (~10 mg/mL), were mixed together at a weight ratio of 1:4:0.5. The PEGylated phospholipids were purchased from Avanti Polar Lipids, Inc., and Laysan Bio Inc. Each mixture was gently stirred for 5−10 min. A Labconco rotory evaporator with a water bath of 25 °C was used to evaporate the organic solvent. The lipidic film, deposited on the reaction vial, was hydrated with 3−5 mL of HPLC water and subjected to ultrasonication for 10−20 min using a bath sonicator. The resulting dispersion was filtered through a 0.45 or 0.2 μm membrane filter and kept at room temperature for further use. To remove the excess phospholipids from the QR dispersion, the micelle-encapsulated QRs were further purified using centrifugation at 10 000 rpm for 15 min. The QR precipitate was then redispersed in 1−2 mL of HPLC water (the water was filtered with a 0.2 mm membrane filter).

D. ***Conjugation of Micelle-Encapsulated QRs with Thiolated RGD.*** A 1 mL portion of a micelle-encapsulated QR stock solution was mixed with 0.5 mL of 1.2 mg/mL of a thiolated RGD peptide solution (the molar ratio of maleimide to RGD peptide is 1:2) and gently stirred for 40−60 min. Next, the resulting bioconjugate dispersion was further purified using centrifugation at 10 000 rpm for 15 min. The QR precipitate was redispersed with 1 mL of HPLC water and kept at 4 °C for further use.

E. ***Spectral Analysis of QRs.*** The absorption spectra of QRs were collected using a Shimadzu model 3101PC UV−vis−near-infrared (NIR) scanning spectrophotometer over a wavelength range from 400 to 900 nm. The samples were measured against chloroform (or water) as the reference. The QR emission spectra were collected using a Fluorolog-3 spectrofluorometer (Jobin Yvon; fluorescence spectra). Solution samples of QRs were filtered through a syringe filter [poly(tetrafluoroethylene), PTFE; pore size 450 nm], diluted to a concentration of about 0.01 g/L, and then loaded into a quartz cuvette for measurements. All of the samples were dispersed in chloroform (or water) and loaded into a quartz cell for measurements. Fluorescence quantum yields (QYs) of the QR dispersions were determined by comparing the integrated emission from the NCs to rhodamine 6G dye solutions of matched absorbance. Samples were diluted so that they were optically thin.

F. ***Particle Size Determination.*** High-resolution transmission electron microscopy (HRTEM) images were obtained using a JEOL model JEM 2010 microscope at an acceleration voltage of 200 kV. The specimens were prepared by drop-coating the sample dispersion onto an amorphous carbon-coated 300 mesh copper grid, which was placed on filter paper to absorb excess solvent. The size distribution and surface potential of micelle-encapsulated QRs were determined by dynamic light scattering (DLS) measurement with a Brookhaven Instruments 90Plus particle size analyzer, with a scattering angle of 90°. For the ζ potential measurement, a phase analysis light scattering module was used.

G. ***Small Animal Imaging Studies.*** Four to five week old nude female mice were purchased from Harlan Sprague Dawley Inc. The animal housing area was maintained at 24 °C with a 12 h light/dark cycle, and animals were fed ad libitum with water and standard laboratory chow. Animal experiments were performed in compliance with guidelines set by the University at Buffalo. All animals were acclimated to the animal facility for at least 48 h prior to experimentation. Tumor model animals were generated by the subcutaneous inoculation (2−3 million cells/100 μL of media) of human pancreatic cancer cell-line Panc-1 (ATCC NO: CRL-1469) in the shoulder of animals using a 1 mL syringe with a 25G needle. After tumor growth to a palpable size, the mice were administered functionalized QRs in 1× PBS by tail vein injection and anesthetized with isoflurane at various time points postinjection. The sedated animals were then imaged using the Maestro in vivo optical imaging system (CRI, Inc., Woburn, MA). Mice were divided into experimental and control groups (five each) in the tumor imaging studies.

H. ***Generation of Orthotopic Xenografts.*** Orthotopic pancreatic cancer xenografts were generated by surgical orthotopic implantation under the pancreatic capsule, as we have previously described (41, 42). Imaging of the primary tumors was performed 4 weeks postimplantation.

RESULTS AND DISCUSSION

The CdSe/CdS/ZnS QRs were prepared by solution-phase synthesis, as described in our previous studies, via growing of a CdS/ZnS graded shell on CdSe rods in a surfactant solution (33). Oleic acid and TOPO were used to passivate the QR surfaces, thereby rendering them dispersible in chloroform. Phospholipid micelles were then used to enable the stable aqueous dispersion, generating a hydrophilic shell with PEG groups on the QR surface (see Scheme 1). For in vivo tumor targeting and imaging studies, an optimized combination of maleimide-functionalized and nonfunctionalized phospholipid PEGs was used to encapsulate the QRs and these encapsulated particles were further conjugated with thiolated cRGD [cyclo(Arg-Gly-Asp-D-Phe-Cys)] to act as biologically targeted luminescent probes.

In this study, the CdSe/CdS/ZnS QRs are coated with coordinating ligands such as hydrophobic moieties (TOPO and oleic acid) and a phospholipid−PEG coating. The strong hydrophobic interactions between hydrophobic surfactants and the phospholipid hydrocarbon chains will produce two oil-like layers that interlock with each other and form a lamellar-like hydrophobic layer surrounding the rod surface, which prevents degradation even under biological fluids (see Scheme 1). As a result, after functionalization with phospholipid−PEG molecules, the encapsulated QRs are protected in such a way that their optical properties (e.g., absorption spectra, emission spectra, and QY) remain unchanged in a broad range of pH (3−10) and temperature conditions (25−70 °C).

Parts a and b of Figure 1 present TEM images of the CdSe/CdS/ZnS QRs in organic media, which are approximately 20.5 nm in length and 4.5 nm in diameter. The lattice fringes of the CdSe/CdS/ZnS QRs are clearly shown in the inset, with fringe spacing of 3.5 Å. Parts c and d of Figure 1 show the phospholipid micelle-encapsulated QRs in aqueous media. A comparison of parts a and b of Figure 1 shows that the size and aspect ratio of the phospholipid micelle-encapsulated CdSe/CdS/ZnS QRs remain unchanged. This suggests that neither aggregation nor "ripening" of the QRs occurs during the phospholipid micelle encapsulation process. From the powder X-ray diffraction pattern of QRs, all of the diffraction peaks correspond to the wurtzite structure of CdSe. HRTEM and powder X-ray diffraction confirmed that the growth axis of the rods was the *c* axis of the wurtzite structure. The water-dispersible, micelle-encapsulated QRs were colloidally stable for more than 3 weeks at 4 °C. Figure 2 shows the UV absorption and photoluminescence (PL) spectra from the monodispersed CdSe/CdS/ZnS QRs. The absorption spectrum features an excitonic peak around 649

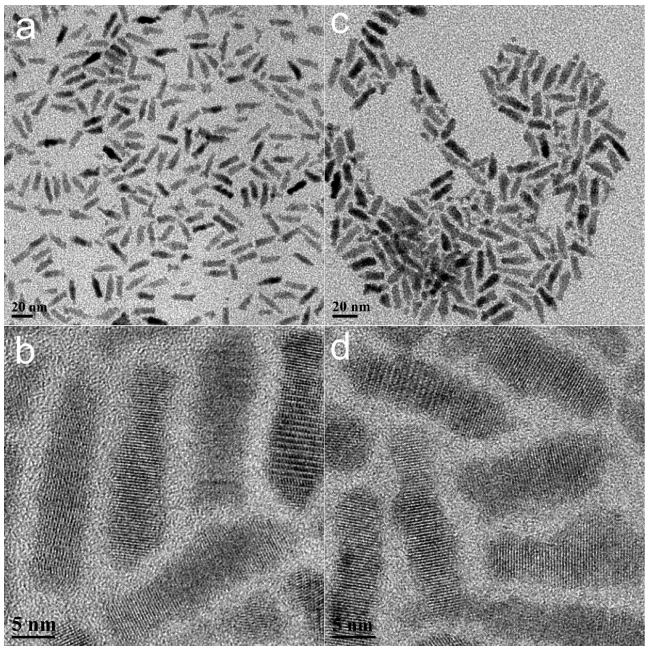

FIGURE 1. TEM images of CdSe/CdS/ZnS QRs dispersed in organic (a and b) and aqueous (c and d) media. The average length and diameter of the nanorods are 20.5 and 4.5 nm, respectively. The aspect ratio of the nanorods is 4.5.

nm. The PL spectrum of the monodispersed QRs shows a band-edge emission at 658 nm. The PL QY of the QRs is estimated to be ~50%. The inset shows a photograph of highly luminescent water-dispersible, micelle-encapsulated QRs exposed by a hand-held UV lamp.

It is favorable to reduce the hydrodynamic size of QR probes for better tumor targeting and imaging (43, 44). We had initially replaced the hydrophobic moiety coating on the QR using thiolated PEG molecules to generate a PEGylated QR with a much smaller size. However, we have observed more than ~80% loss of their PL intensity immediately, and a further loss of the PL intensity was observed after 1−2 days of storage at room temperature. This strongly indicates that the QRs are very sensitive toward any ligand exchange process, thereby justifying our strategy of using the phospholipid−PEG encapsulation approach to prevent the breakdown of QR.

DLS was used to determine the hydrodynamic size and colloidal stability of the QRs dispersed in PBS (pH = 7.4). The DLS measurement shows that the engineered QR probes have hydrodynamic radii of ~32 nm (see Figure 2b). Over the time range from 0 to 3 days, the effective radius varies by less than 20%, suggesting that their colloidal stability is not affected under physiological pH. It has been recently reported that PEGylated colloidal gold nanoparticles with hydrodynamic radii of 40−50 nm did not cause any difficulties for in vivo tumor imaging (45).

Prior to in vivo tumor imaging, a body weight evaluation was performed on mice injected intravenously with the QRs in order to assess the signs of potential toxicity (46). The body weight change is a useful indicative parameter for studying the acute toxic effects of administered nanoparticles in animals (47). In this experiment, BALB/c mice were divided into two groups (five mice per group), with one group receiving 1 mg of micelle-encapsulated QRs and the other group not receiving any injection. No significant differences in the average body weight between these two groups were observed for more than 1 week after treatment of the micelle-encapsulated QRs. Also, physical evaluations of the QR-treated mice did not indicate any changes in eating, drinking, exploratory behavior, and physical features (e.g., hair color). These preliminary studies indicate nontoxicity of these QRs in vivo, particularly in the short term.

The maleimide-functionalized-phospholipid, micelle-encapsulated QRs are conjugated with thiolated cRGD peptides for in vivo tumor targeting. These maleimide-functionalized QRs have roughly 200 maleimide groups on the surface of each QR. The maleimine groups on the particle surface were roughly estimated based on the following assumption: we first assume a close-packed monolayer of mixed surfactants (TOPO and oleic acid) on the surface of QR. In this case, the total numner of surfactants attached on a nanoparticle is $4\pi r^2/\alpha$, where r is the radius of the particle and α is the head area per molecule of the surfactant. Here, it is assumed that the surfactants, TOPO and oleic acid, are adsorbed to the QD surface to an equal extent and their average head packing area is 21 Å^2 (α), as is usually calculated for similar amphiphilic molecules. Also, we assume that each surfactant can only interact with one PEGylated phospholipid molecule. Thus, one can finally determine the number of maleimide groups on the QD surface by including the final concentration fraction of DSPE-PEG-maleimide in the calculation. In this study, a large excess of the thiolated cRGD was used for conjugation and we estimated that there are at least 150−200 cRGD peptides per QR based on the conjugation efficiency of the maleimide groups. The number of cRGD peptides per rod is at least 3−4 times greater than that of the dot particle. To visualize the synthesized QR bioconjugate, we again performed TEM on QR conjugated with cRGD. Specimens were prepared by drop-casting a QR bioconjugate solution onto the TEM grid, and the size of the QR bioconjugates measured by TEM was similar to that of nonconjugated QRs (data not shown). The TEM analysis clearly indicated that the QR bioconjugates are monodispersed and do not show any sign of agglomeration or aggregation. The QR bioconjugates were colloidally and optically stable for 1 week in a PBS buffer.

For an in vivo whole body tumor imaging study, athymic nude mice bearing subcutaneous Panc-1 tumors [3−4 weeks postinoculation of (2−3) × 10^6 Panc-1 cells on the left shoulder, at a tumor size of about ~0.5−0.9 cm^3] were injected (intravenously) with nonbioconjugated or cRGD-conjugated QRs (~1 mg of QR bioconjugates per animal; number of mice = 5). The mice were imaged at different time points starting from 1 to 24 h postinjection using the Maestro in vivo imaging system (CRI, Inc., Woburn, MA; excitation filter = 445−490 nm, emission filter = 515-nm-long pass). The Maestro optical system consists of an optical head that includes a liquid-crystal tunable filter (with a bandwidth of 20 nm and a scanning wavelength range of 500−950 nm) with a custom-designed,

Scheme 1. Schematic Illustration Showing the Formation of the Water-Dispersible CdSe/CdS/ZnS QR Bioconjugates

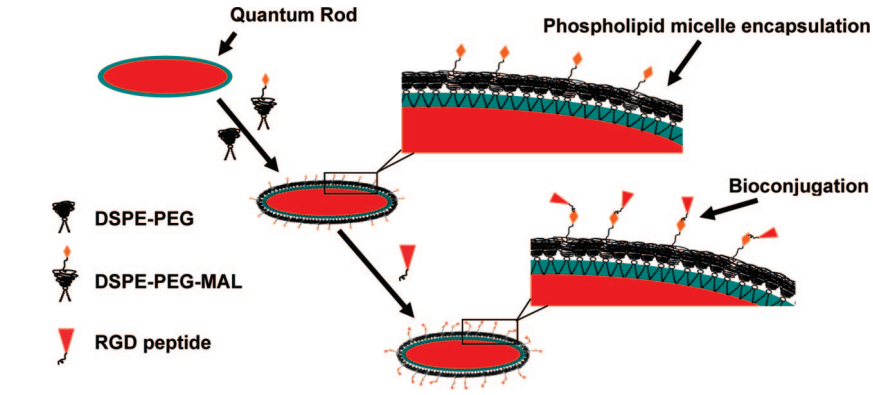

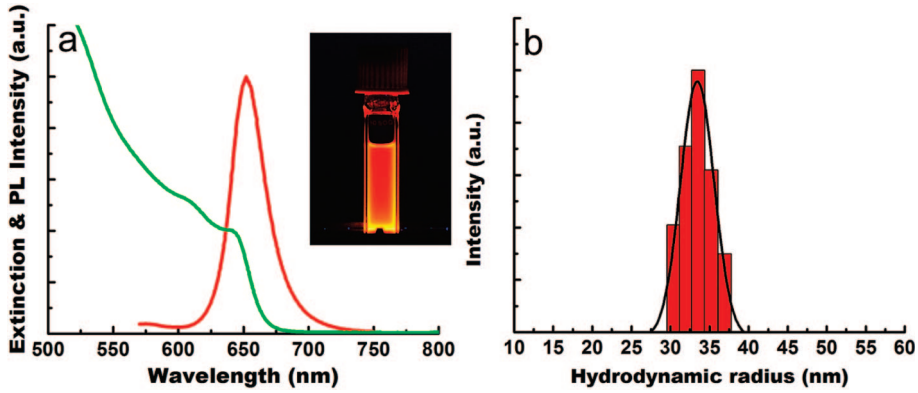

FIGURE 2. (a) UV−vis absorption (green) and PL (red) spectra of monodispersed CdSe/CdS/ZnS QRs. (b) DLS plot of monodispersed micelle-encapsulated QRs.

spectrally optimized lens system that relays the image to a scientific-grade megapixel CCD. The CCD captured the images at each wavelength. The captured images (spectral cube, containing a spectrum at every pixel) can be loaded into the vendor software and analyzed. Spectra from the autofluorescence (from the skins, tissues, and food, coded green) and QR-associated luminescence signals (coded red) can be unmixed using the vendor software, as shown in Figure 3. In this study, the scanning wavelength range between 500 and 900 nm was used as recommended by the CRI, Inc., instrument manual.

Figure 4 shows the in vivo luminescent imaging of Panc-1 tumor-bearing mice (in the left shoulder as indicated by white arrows) injected with ~1 mg of cRGD-conjugated QR (panels a−f) and nonconjugated QR (panels m−r), respectively. All images were acquired using the same instrumental conditions. It can be seen that, within 1 h of postinjection, a strong luminescence signal was detected in the Panc-1 tumor. During the next 23 h, a steady decrease in the tumor luminescent intensity in tumor-bearing mice treated with QR bioconjugates can be observed (see Figure 4, panels a−f), with almost no discernible signal even at 18 h postinjection. Figure 5 shows the lateral view of the QR-cRGD-treated Panc-1 tumor-bearing mice. These figures correspond to panels a−f in Figure 4. In control experiments, no detectable luminescent signal was observed in the tumor for the nonbioconjugated-QR-injected mice (number of mice = 5), at any time point postinjection (Figure 4, panels m−r),

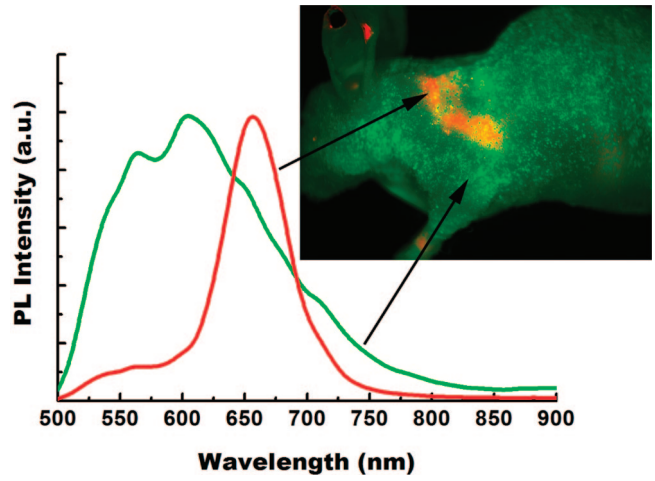

FIGURE 3. Unmixing spectra of autofluorescence (green) and QR (red) from a tumor-bearing nude mouse treated with QR bioconjugates. The QR spectrum was obtained by subtraction of the autofluorescence signal from the mixture signal of the mouse treated with QR bioconjugates.

indicating their poor tumor specificity. These results validate the high-efficiency tumor targeting of cRGD-conjugated, as opposed to nonbioconjugated, QRs in vivo. It is worth mentioning that the QR concentration used here is at least 6.5 times higher than that reported previously for in vivo imaging using other QDs (48). This demonstrates the biocompatibility and negligible in vivo toxicity of the engineered QRs for in vivo applications.

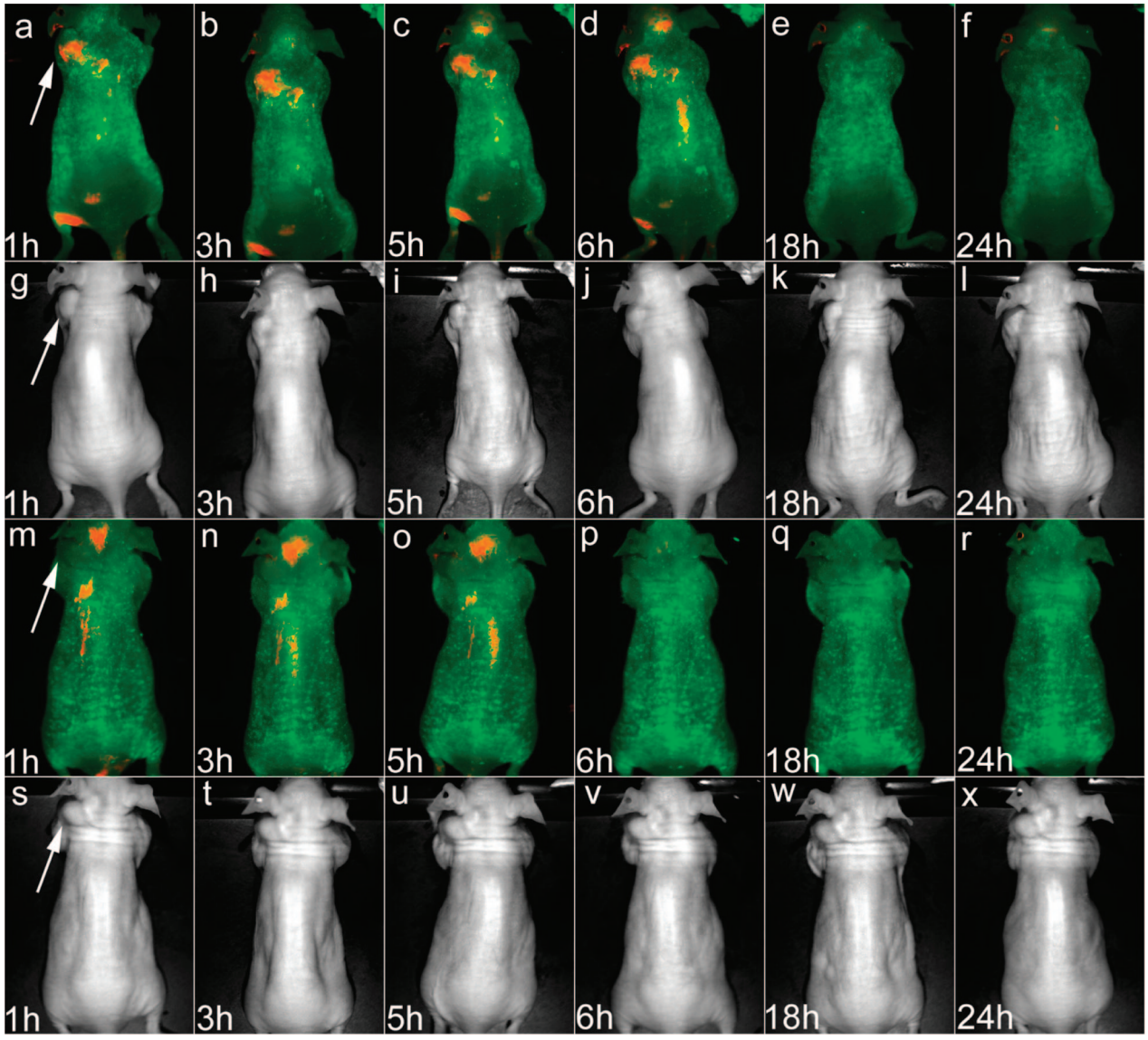

FIGURE 4. Time-dependent in vivo luminescence imaging of Panc-1 tumor-bearing mice (left shoulder, indicated by white arrows) injected with ~1 mg of cRGD-peptide-conjugated QRs (panels a–f) and nonconjugated QRs (panels m–r), respectively. All images were acquired under the same experimental conditions. The autofluorescence from tumor-bearing mice is coded in green, and the unmixed QR signal is coded in red. Prominent uptake in the liver, spleen, and lymph nodes was also visible. TEM images in panels g–i and panels s–x correspond to the luminescence images in panels a–f and panels m–r, respectively.

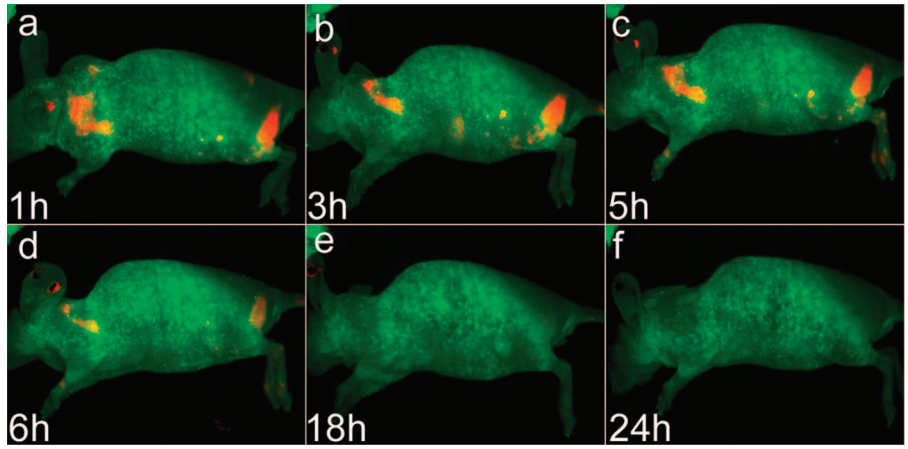

FIGURE 5. Lateral view of in vivo luminescence imaging of Panc-1 tumor-bearing mice (left shoulder) injected with ~1 mg of cRGD-peptide-conjugated QRs. These images correspond to the images taken in Figure 4, panels a–f.

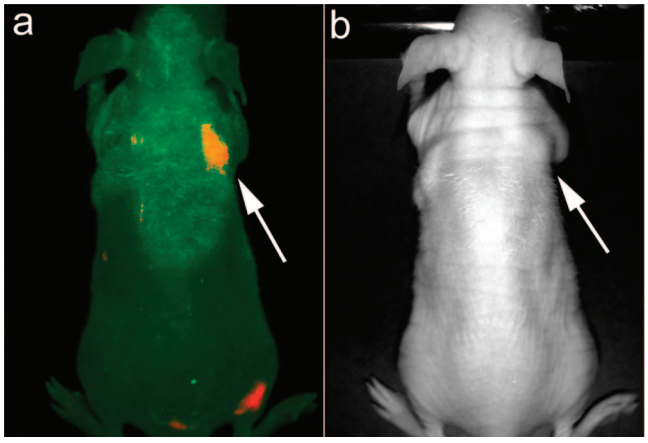

FIGURE 6. In vivo luminescence imaging of mice at 2 weeks postinoculation of Panc-1 cancer cells subcutaneously (right shoulder, indicated by white arrows) injected with ~0.5 mg of cRGD-peptide-conjugated QRs. The autofluorescence from tumor-bearing mice is coded in green, and the unmixed QR signal is coded in red. The TEM image in part b corresponds to the luminescence image in part a.

To further prove that the engineered QRs can be used for early cancer detection, nude mice with 2 weeks postinoculation of (2−3) × 10^6 Panc-1 cells on their right shoulder (early stage of the tumor growth) were injected intravenously with the same QR-cRGD bioconjugates. Similar to that observed using bigger tumors (Figures 4 and 5), Figure 6 shows a strong luminescence signal emanating from the site of inoculation of tumor cells, thus demonstrating the ability of QR-cRGD bioconjugates to successfully enable targeted bioimaging of tumors during angiogenesis seen in the early development of the tumor.

To examine the distribution of functionalized QRs in tumor-bearing mice, they were sacrificed and major organs were removed for luminescence imaging after intravenous injection with QR bioconjugates for 72 h (see Figure 7). Luminescence images of the heart, liver, spleen, lung, and kidney were obtained from tumor-bearing mouse after tail vein injection of functionalized QRs. As observed from the characteristic red luminescence of QRs, cRGD-functionalized QR uptake took place primarily in the liver and spleen, with little or no QR accumulation in the heart, kidney, and lung. We noted that accumulation of QRs in the liver and spleen was reduced with time. This pattern of in vivo organ distribution from small animals is similar to that of functionalized QD targeted probes previously reported (48, 49).

In addition to using mice bearing subcutaneous xenografts of pancreatic cancer, we have also carried out preliminary targeted bioimaging studies in mice orthotopically implanted with human pancreatic cancer. In contrast to subcutaneous xenografts, orthotopic tumors, particularly those in the pancreas, simulate the pitfalls of in vivo targeted imaging in humans because of their proximity to the hepatic and splenic fields, with the latter being typical sources of artifactual fluorescence due to reticuloendothelial uptake (see below). A demonstration of optimal imaging parameters in the orthotopic setting, thus, provides a considerably higher degree of confidence in the path toward clinical translation, not accorded by conventional subcutaneous tumors. It is also worth noting that the pattern of tumor angiogenesis in orthotopic primaries is more likely to recapitulate the cognate human disease than the pattern arising in subcutaneous xenografts, a matter of not insignificant consideration when using a vascular targeted imaging strategy. Figure 8a shows the luminescence images of a dissected mouse bearing orthotopic pancreatic cancer xenografts, following 2 h of intravenous injection of cRGD QRs. From the figure, the successful targeting of the orthotopic tumor can be visualized by the characteristic red emission associated with the QRs. Parts b and c of Figure 8 compare the images of the resected orthotopic tumors from mice injected with cRGD-targeted, as opposed to nonbioconjugated, QRs. The observation of red emission from the tumors of mice receiving targeted QRs, but not from that of mice receiving nonbioconjugated QRs, indicates that cRGD conjugation is necessary for specifically targeting the QRs to orthotopic tumors in vivo.

For in vivo application, it is important to reduce QR uptake by the RES. It is widely known in the field of targeted delivery that the functionalization of an outer layer of PEG on nanoparticles endows the nanoparticles with RES-evading properties. This increases the circulation time of the nanoparticles in blood, thereby enhancing their ability to accumulate in solid tumors by passive diffusion, with the help of the enhanced permeability and retentivity effect. In this study, we have observed that, by incorporation of PEG into the QR bioconjugates, a reduced uptake in the liver, spleen, and bone marrow was observed upon comparison to other studies. However, without the cRGD peptide conjugated to the surface, little to no tumor accumulation of the PEG−phospholipid-coated QRs was observed. Previous reports have mentioned that long PEG-functionalized QDs may likely reduce the probability of QDs to target the tumor cells because of substantially increased particle sizes. However, this scenario did not occur in our studies.

The above experiments successfully demonstrate that cRGD-conjugated QRs can be used for targeted delivery and imaging of both subcutaneous and orthotopic tumors in vivo. To the best of our knowledge, this is the first successful demonstration of functionalized QRs for in vivo tumor targeting and imaging. The unique properties of the QRs can be combined with advances in targeted diagnostics and therapeutics, thus paving the way for numerous novel biomedical applications involving QR bioconjugates. Recently, we have reported the use of CdSe/CdS/ZnS QRs for multiplex labeling of live human cancer cells using a single excitation source (50). This technique was used to image human pancreatic cancer in vitro, by conjugating QRs with the monoclonal antibodies anticlaudin 4 or antimesothelin, which target the claudin 4 and mesothelin receptors overexpressed on pancreatic cancer. Therefore, it might be worth exploring the conjugation of different potential tumor targeting agents with QRs emitting in two or more colors for the simultaneous evaluation of the tumor specificity of these agents in vivo. We are currently in the process of investigating whether the different aspect ratios of QRs can give an

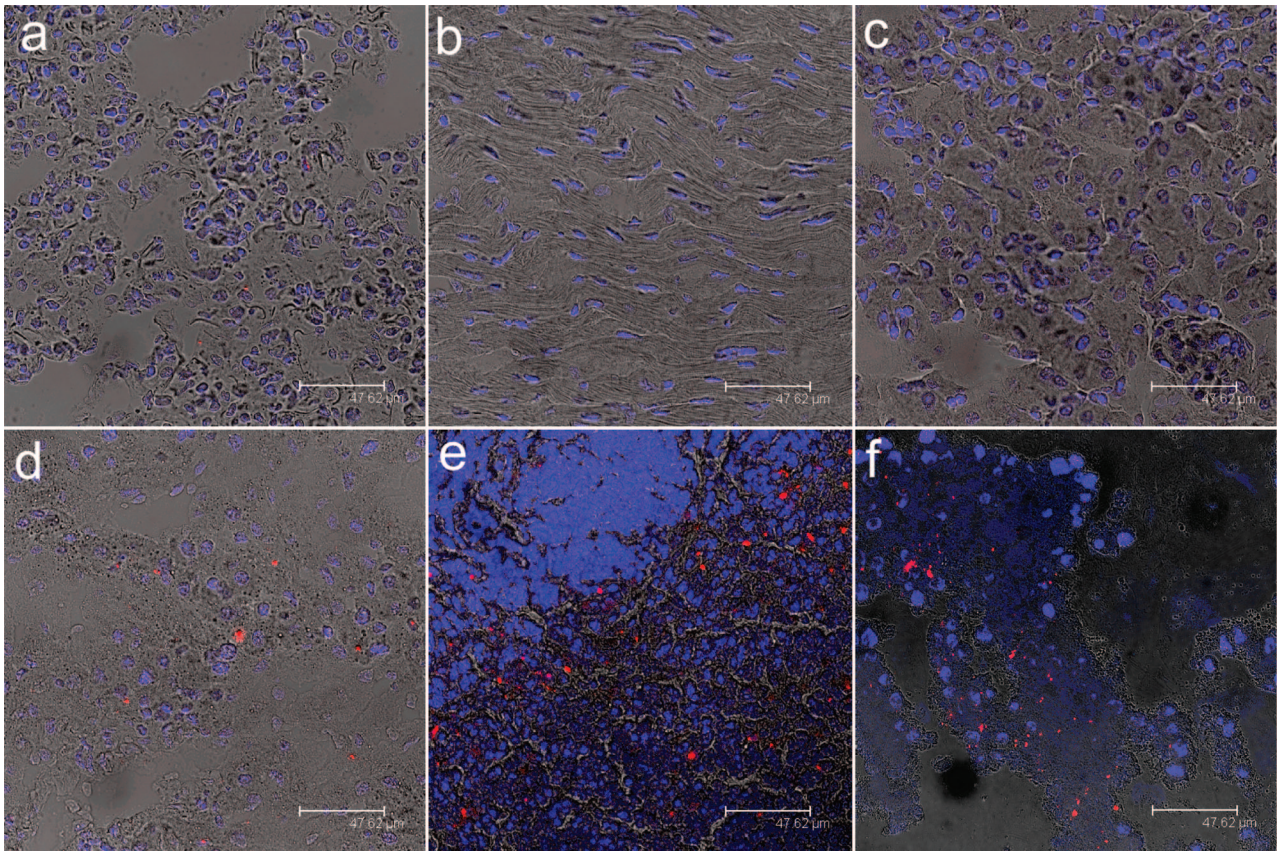

FIGURE 7. Tissue sections from Panc-1 tumor-bearing mice intravenously injected with cRGD peptide-conjugated CdSe/CdS/ZnS QRs. Tissues were harvested from the lung (a), heart (b), kidney (c), liver (d), spleen (e), and tumor (f). In all cases, blue represents emission from Hoechst 33342 and red represents emission from functionalized CdSe/CdS/ZnS QRs.

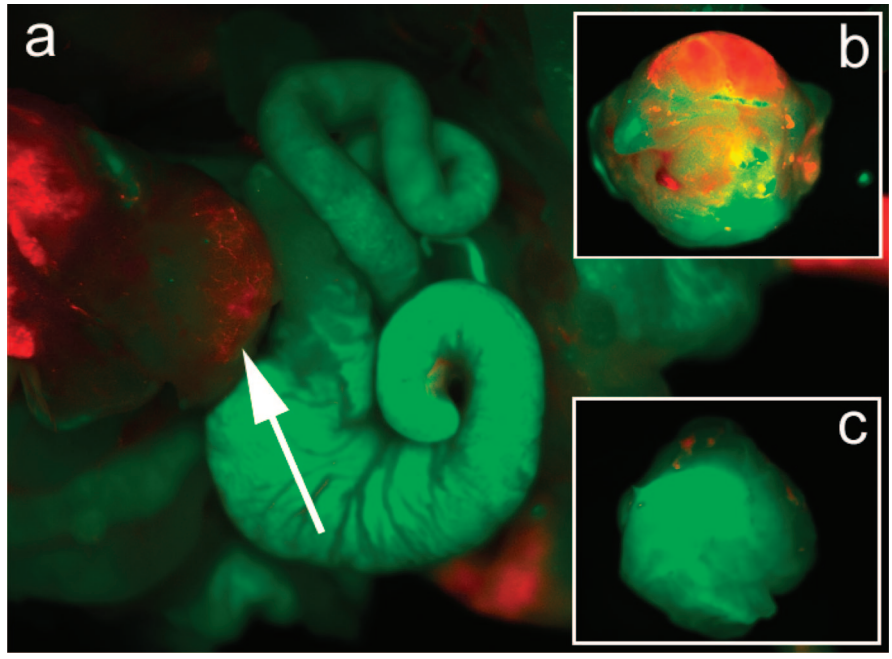

FIGURE 8. (a) In vivo luminescence imaging of an orthotopic tumor model mouse (the tumor is indicated by a white arrow) injected with ~1 mg of cRGD-peptide-conjugated QRs. The autofluorescence from mice is coded in green, and the unmixed QR signal is coded in red. (b) Ex vivo orthotopic tumor luminescent images of nonconjugated QRs and (c) cRGD-conjugated QRs harvested from mice at 2 h postinjection. The autofluorescence from the tumor is coded in green, and the unmixed QR signal is coded in red.

extra degree of freedom to improve targeting efficiency and better in vivo imaging capability. In addition, multiple biomolecules can be conjugated to the large surface area of QR (per particle) to target multiple receptors on the tumor sites (51). For example, a combination of monoclonal antibodies (anticlaudin 4 or anti mesothelin) and RGD peptides can be

used to modify the surface of micelle-encapsulated QRs for simultaneous in vivo labeling of the tumor mass and the surrounding vasculature of pancreatic cancer, respectively.

In addition to UV−vis-range-emitting QRs, QRs such as CdTe/CdSe/ZnS that emit at the NIR region may be a good alternative for in vivo tumor imaging especially in human studies because autofluorescence and light absorbance of biological specimens in the NIR regions are at their minimum (52, 53). Also, multimodality imaging of QR-based probes can be fabricated using a solution-phase synthesis method (47). For example, QRs can be incorporated with paramagnetism, and this multimodal QR will allow noninvasive tumor diagnosis using combined optical and magnetic resonance imaging scans. The high QY, together with the NIR-emitting luminescent wavelength and paramagnetism within one single multimodal QR probe, makes it particularly attractive and promising for in vivo early cancer detection (54, 55), where the exact location and dimensions of the tumor can be pinpointed precisely using concurrent magnetic resonance and NIR luminescent imaging.

The low-toxicity, micelle-encapsulated QR probes developed here may provide a nanoplatform for early detection of human pancreatic cancer. Cancer of the pancreas is the fourth leading cause of cancer-related mortality in the United States and accounts for more than 31 000 deaths each year (56). The vast majority of patients present with locally advanced or distant metastatic disease, rendering the cancer inoperable. Current drug and radiation therapies have been ineffective in ameliorating the prognosis of this uniformly lethal disease. Therefore, in order to improve the survival rate of pancreatic cancer patients, ultrasensitive imaging probes are needed for diagnosing pancreatic cancer at an early, and hence potentially curative, stage. We believe that the current work will serve as an important milestone for future in vivo studies aimed at an early detection of pancreatic cancer, where better tumor-locating efficiency can be achieved. Also, we envisioned that in those patients where early pancreatic cancer detection is achieved using QRs more successful surgical intervention can be performed by optically guided surgery. This necessitates the removal of all cancerous areas surrounding the tumor site without harming the normal tissue.

CONCLUSION

In summary, we have demonstrated that cRGD-peptide-conjugated, micelle-encapsulated QRs can be used as targeted probes for labeling cancer in vivo, using both subcutaneous and orthotopic models of pancreatic cancer bearing mice. Because tumor vasculatures are overexpressesed with $\alpha_V\beta_3$ integrin, cRGD QR bioconjugates can be served as a new class of anisotropic nanoparticle-based probes for early detection and imaging of cancer in vivo. More importantly, these probes are able to selectively target and image early tumor growth. The results reported here may aid in the advancement of $\alpha_V\beta_3$ integrin-targeted luminescent imaging using anisotropic semiconductor nanoparticles and will have great potential for traceable drug delivery cancer therapy.

Acknowledgment. This study was supported by grants from the NCI (Grants CA119397, CA119358, and CA104492) and the John R. Oishei Foundation. K.-T.Y. is supported by the AACR−Pancreatic Cancer Action Network Fellowship for Pancreatic Cancer Research. K.-T.Y. is grateful to the reviewers for their helpful comments.

REFERENCES AND NOTES

(1) Hull, K. L.; Grebinski, J. W.; Kosel, T. H.; Kuno, M. *Chem. Mater.* **2005**, *17* (17), 4416–4425.
(2) Li, C.; Curreli, M.; Lin, H.; Lei, B.; Ishikawa, F. N.; Datar, R.; Cote, R. J.; Thompson, M. E.; Zhou, C. *J. Am. Chem. Soc.* **2005**, *127* (36), 12484–12485.
(3) Morales, A. M.; Lieber, C. M. *Science* **1998**, *279* (5348), 208–211.
(4) Shi Kam, N. W.; O'Connell, M.; Wisdom, J. A.; Dai, H. *Proc. Natl. Acad. Sci. U.S.A.* **2005**, *102* (33), 11600–11605.
(5) Trentler, T. J.; Hickman, K. M.; Goel, S. C.; Viano, A. M.; Gibbons, P. C.; Buhro, W. E. *Science* **1995**, *270* (5243), 1791–1794.
(6) Tuan, H. Y.; Lee, D. C.; Hanrath, T.; Korgel, B. A. *Nano Lett.* **2005**, *5* (4), 681–684.
(7) Kuno, M.; Ahmad, O.; Protasenko, V.; Bacinello, D.; Kosel, T. H. *Chem. Mater.* **2006**, *18* (24), 5722–5732.
(8) Panda, A. B.; Glaspell, G.; El-Shall, M. S. *J. Am. Chem. Soc.* **2006**, *128*, 2790–2791.
(9) Saunders, A. E.; Popov, I.; Banin, U. *J. Phys. Chem. B* **2006**, *110* (50), 25421–25429.
(10) Yong, K. T.; Sahoo, Y.; Choudhury, K. R.; Swihart, M. T.; Minter, J. R.; Prasad, P. N. *Nano Lett.* **2006**, *6* (4), 709–714.
(11) Yong, K. T.; Sahoo, Y.; Choudhury, K. R.; Swihart, M. T.; Minter, J. R.; Prasad, P. N. *Chem. Mater.* **2006**, *18* (25), 5965–5972.
(12) Yong, K. T.; Sahoo, Y.; Swihart, M. T.; Prasad, P. N. *J. Phys. Chem. C* **2007**, *111* (6), 2447–2458.
(13) Yong, K.-T.; Sahoo, Y.; Swihart, M. T.; Prasad, P. N. *Adv. Mater.* **2006**, *18*, 1978–1982.
(14) Yong, K. T.; Sahoo, Y.; Zeng, H.; Swihart, M. T.; Minter, J. R.; Prasad, P. N. *Chem. Mater.* **2007**, *19* (17), 4108–4110.
(15) Kim, W.; Ng, J. K.; Kunitake, M. E.; Conklin, B. R.; Yang, P. *J. Am. Chem. Soc.* **2007**, *129* (23), 7228–7229.
(16) Prasad, P. N. *Nanophotonics*; Wiley-Interscience: New York, 2004.
(17) Bierman, M. J.; Lau, Y. K. A.; Jin, S. *Nano Lett.* **2007**, *7* (9), 2907–2912.
(18) Manna, L.; Milliron, D. J.; Meisel, A.; Scher, E. C.; Alivisatos, A. P. *Nat. Mater.* **2003**, *2* (6), 382–385.
(19) Yin, Y.; Alivisatos, A. P. *Nature* **2005**, *437* (7059), 664–670.
(20) Yong, K.-T.; Sahoo, Y.; Swihart, M.; Schneeberger, P.; Prasad, P. *Top. Catal.* **2008**, *47* (1), 49–60.
(21) Burda, C.; Chen, X.; Narayanan, R.; El-Sayed, M. A. *Chem. Rev.* **2005**, *105* (4), 1025–1102.
(22) Peng, Z. A.; Peng, X. *J. Am. Chem. Soc.* **2001**, *123* (1), 183–184.
(23) Peng, Z. A.; Peng, X. *J. Am. Chem. Soc.* **2001**, *123* (7), 1389–1395.
(24) Peng, Z. A.; Peng, X. *J. Am. Chem. Soc.* **2002**, *124* (13), 3343–3353.
(25) Talapin, D. V.; Mekis, I.; Gotzinger, S.; Kornowski, A.; Benson, O.; Weller, H. *J. Phys. Chem. B.* **2004**, *108*, 18826–18831.
(26) Prasad, P. N. *Biophotonics*; Wiley-Interscience: New York, 2004.
(27) Huang, X.; El-Sayed, I. H.; Qian, W.; El-Sayed, M. A. *J. Am. Chem. Soc.* **2006**, *128* (6), 2115–2120.
(28) Alivisatos, P. *Nat. Biotechnol.* **2004**, *22* (1), 47–52.
(29) Huynh, W. U.; Dittmer, J. J.; Alivisatos, A. P. *Science* **2002**, *295* (5564), 2425–2427.
(30) Mokari, T.; Banin, U. *Chem. Mater.* **2003**, *15*, 3955–3960.
(31) Peng, X.; Manna, L.; Yang, W.; Wickham, J.; Scher, E.; Kadavanich, A.; Alivisatos, A. P. *Nature* **2000**, *404* (6773), 59–61.
(32) Fu, A.; Gu, W.; Boussert, B.; Koski, K.; Gerion, D.; Manna, L.; LeGros, M.; Larabell, C. A.; Alivisatos, A. P. *Nano Lett.* **2007**, *7* (1), 179–182.
(33) Yong, K. T.; Qian, J.; Roy, I.; Lee, H. H.; Bergey, E. J.; Tramposch, K. M.; He, S.; Swihart, M. T.; Maitra, A.; Prasad, P. N. *Nano Lett.* **2007**, *7* (3), 761–765.
(34) Dubertret, B.; Skourides, P.; Norris, D. J.; Noireaux, V.; Brivanlou, A. H.; Libchaber, A. *Science* **2002**, *298* (5599), 1759–1762.
(35) Gil, P. R.; Parak, W. J. *ACS Nano* **2008**, *2* (11), 2200–2205.
(36) Rajangam, K.; Behanna, H. A.; Hui, M. J.; Han, X.; Hulvat, J. F.; Lomasney, J. W.; Stupp, S. I. *Nano Lett.* **2006**, *6* (9), 2086–2090.

(37) Cheng, Z.; Wu, Y.; Xiong, Z.; Gambhir, S. S.; Chen, X. *Bioconjugate Chem.* **2005**, *16* (6), 1433–1441.
(38) Cai, W.; Shin, D. W.; Chen, K.; Gheysens, O.; Cao, Q.; Wang, S. X.; Gambhir, S. S.; Chen, X. *Nano Lett.* **2006**, *6* (4), 669–676.
(39) Zhou, M.; Ghosh, I. *Pept. Sci.* **2007**, *88* (3), 325–339.
(40) Manna, L.; Scher, E. C.; Li, L.-S.; Alivisatos, A. P. *J. Am. Chem. Soc.* **2002**, *124* (24), 7136–7145.
(41) Feldmann, G.; Dhara, S.; Fendrich, V.; Bedja, D.; Beaty, R.; Mullendore, M.; Karikari, C.; Alvarez, H.; Iacobuzio-Donahue, C.; Jimeno, A.; Gabrielson, K. L.; Matsui, W.; Maitra, A. *Cancer Res.* **2007**, *67* (5), 2187–2196.
(42) Feldmann, G.; Fendrich, V.; McGovern, K.; Bedja, D.; Bisht, S.; Alvarez, H.; Koorstra, J.-B. M.; Habbe, N.; Karikari, C.; Mullendore, M.; Gabrielson, K. L.; Sharma, R.; Matsui, W.; Maitra, A. *Mol. Cancer Ther.* **2008**, *7* (9), 2725–2735.
(43) Soo Choi, H.; Liu, W.; Misra, P.; Tanaka, E.; Zimmer, J. P.; Itty Ipe, B.; Bawendi, M. G.; Frangioni, J. V. *Nat. Biotechnol.* **2007**, *25* (10), 1165–1170.
(44) Liu, W.; Choi, H. S.; Zimmer, J. P.; Tanaka, E.; Frangioni, J. V.; Bawendi, M. *J. Am. Chem. Soc.* **2007**, *129* (47), 14530–14531.
(45) Qian, X.; Peng, X.-H.; Ansari, D. O.; Yin-Goen, Q.; Chen, G. Z.; Shin, D. M.; Yang, L.; Young, A. N.; Wang, M. D.; Nie, S. *Nat. Biotechnol.* **2008**, *26* (1), 83–90.
(46) Chen, H.; Wang, Y.; Xu, J.; Ji, J.; Zhang, J.; Hu, Y.; Gu, Y. *J. Fluoresc.* **2008**, *18* (5), 801–811.
(47) Yong, K.-T. *Nanotechnology* **2009**, *20* (1), 015102.
(48) Gao, X.; Cui, Y.; Levenson, R. M.; Chung, L. W. K.; Nie, S. *Nat. Biotechnol.* **2004**, *22* (8), 969–976.
(49) Akerman, M. E.; Chan, W. C. W.; Laakkonen, P.; Bhatia, S. N.; Ruoslahti, E. *Proc. Natl. Acad. Sci. U.S.A.* **2002**, *99* (20), 12617–12621.
(50) Yong, K.-T.; Roy, I.; Pudavar, H. E.; Bergey, E. J.; Tramposch, K. M.; Swihart, M. T.; Prasad, P. N. *Adv. Mater.* **2008**, *20* (8), 1412–1417.
(51) Xu, G.; Yong, K.-T.; Roy, I.; Mahajan, S. D.; Ding, H.; Schwartz, S. A.; Prasad, P. N. *Bioconjugate Chem.* **2008**, *19* (6), 1179–1185.
(52) Kim, S.; Lim, Y. T.; Soltesz, E. G.; De Grand, A. M.; Lee, J.; Nakayama, A.; Parker, J. A.; Mihaljevic, T.; Laurence, R. G.; Dor, D. M.; Cohn, L. H.; Bawendi, M. G.; Frangioni, J. V. *Nat. Biotechnol.* **2004**, *22* (1), 93–97.
(53) Michalet, X.; Pinaud, F. F.; Bentolila, L. A.; Tsay, J. M.; Doose, S.; Li, J. J.; Sundaresan, G.; Wu, A. M.; Gambhir, S. S.; Weiss, S. *Science* **2005**, *307* (5709), 538–544.
(54) Kim, J.; Kim, K. S.; Jiang, G.; Kang, H.; Kim, S.; Kim, B.-S.; Park, M. H.; Hahn, S. K. *Biopolymers* **2008**, *89* (12), 1144–1153.
(55) Manzoor, K.; Johny, S.; Thomas, D.; Setua, S.; Menon, D.; Nair, S. *Nanotechnology* **2009**, *20* (6), 065102.
(56) Karikari, C. A.; Roy, I.; Tryggestad, E.; Feldmann, G.; Pinilla, C.; Welsh, K.; Reed, J. C.; Armour, E. P.; Wong, J.; Herman, J.; Rakheja, D.; Maitra, A. *Mol. Cancer Ther.* **2007**, *6* (3), 957–966.

AM8002318